JOURNAL OF EXPERIMENTAL AND THEORETICAL PHYSICS, 2024, Vol. 166, No. 6 (12), pp. 847–856

ELECTRONIC PROPERTIES OF SOLID

WIGNER CRYSTALLIZATION IN TWO-DIMENSIONAL STRUCTURES IN MAGNETIC FIELD. ACOUSTIC STUDIES

© 2024 I. L. Drichko[a], I. Yu. Smirnov[a]*, A. V. Suslov[b], D. R. Leadley[c], Yu. M. Galperin[d,a]

[a] A.F. Ioffe Physico-Technical Institute of the Russian Academy of Sciences, Saint Petersburg, 194021 Russia
[b] National High Magnetic Field Laboratory Tallahassee, FL 32310, USA
[c] Department of Physics, University of Warwick Coventry CV4 7AL, United Kingdom
[d] University of Oslo 0316 Oslo, Norway
* e-mail: ivan.smirnov@mail.ioffe.ru

Received June 05, 2024
Revised June 05, 2024
Accepted June 26, 2024

Abstract. A review of studies on Wigner crystallization in two-dimensional structures using acoustic methods is presented. These methods allowed determining the frequency dependencies of the real σ_1 and imaginary σ_2 components of high-frequency conductivity $\sigma^{hf} = \sigma_1 - i\sigma_2$. Charge carrier crystallization was observed at low temperatures $T < 0.3$ K in strong magnetic fields near filling factors $\nu \leqslant 2$. The frequency dependencies of real σ_1 and imaginary σ_2 conductivity components make it possible to establish the formation of Wigner crystal domains in structures, calculate their average sizes, and determine the melting temperature.

The article is presented as part of the proceedings of the 39th Conference on Low Temperature Physics (LT-2024), Chernogolovka, June 2023

DOI: 10.31857/S004445102412e101

1. INTRODUCTION

The possibility of electron crystal formation was theoretically predicted by Wigner in 1937 [1]. In 1972, Chaplik [2] investigated the formation of Wigner crystal in an inversion layer with low electron concentration and calculated sound wave absorption for such a system. In 1975, Lozovik and Yudson [3] noted that in two-dimensional systems, a strong magnetic field can lead to electron crystallization even at such high carrier concentrations where the formation of a Wigner crystal in zero field is impossible.

The first report of the emergence of a Wigner crystal on the surface of liquid helium was made in 1979 [4]. Subsequently, anomalies observed in the temperature dependencies of resistance in two-dimensional structures at very low temperatures in strong magnetic fields began to be explained by the formation of Wigner crystal domains pinned on disorder – Wigner glass. While the influence of Wigner crystal domains on resistance was studied mainly in two-dimensional GaAs/AlGaAs structures, as these structures possessed the highest mobility and low carrier concentration (see reviews [5, 6], and references therein), Pudalov's group conducted research on structures Si/SiO_2, the results of which are presented in [7]. The listed works mainly used DC techniques. In our research, we used acoustic methods that enable the study of dynamic properties of two-dimensional structures with Wigner crystal domains (Wigner glass), specifically: high-frequency conductivity. In this work, we will focus precisely on the investigation of these properties, conducted by our group over different years and on various two-dimensional objects. High-frequency conductivity was first studied by acoustic methods in *n*-GaAs/AlGaAs structures in the Wigner crystallization regime using acoustic methods in works [8].

Naturally, numerous theoretical works were devoted to this problem, references to which are presented in [9] and reviews [5, 6]. In this work, we will very briefly trace the main developments in the

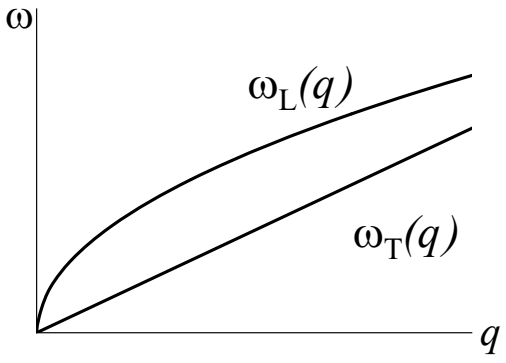

Fig. 1. 1. Schematic representation of phonon modes in a two-dimensional Wigner crystal as in work [9]. Pure two-dimensional Wigner crystal at zero magnetic field: longitudinal phonon mode (plasmon) and transverse (shear) phonon mode

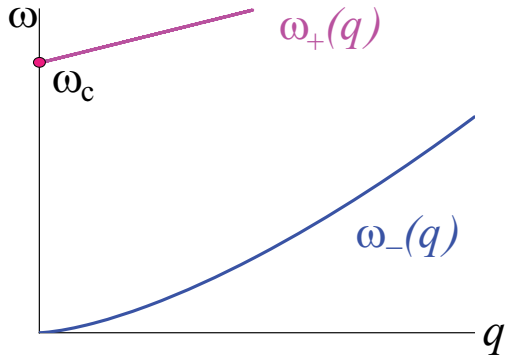

Fig. 2. Pure two-dimensional Wigner crystal in a perpendicular magnetic field: magnetoplasmon ($\omega_+(q)$) and magnetophonon ($\omega_-(q)$) modes

theory devoted to Wigner crystallization in two-dimensional structures.

2. THEORY

For the formation of a Wigner crystal, the following condition must be met: the Coulomb interaction energy E_{ee} must exceed the Fermi energy E_F. In a two-dimensional electron (hole) system

$$E_{ee} \gg E_F, \qquad \frac{(\pi n_s)^{1/2} e^2}{\varepsilon} \gg \frac{\pi \hbar^2 n_s}{m^*},$$

$$\kappa_s = \frac{E_{ee}}{E_F} \gg 1.$$

If we consider the Wigner crystal as an elastic continuum, it is characterized by elastic moduli (bulk λ and shear β), mass density and lattice constant. All these values are determined by the electron concentration. Below we will consider the formation of Wigner crystals in three different situations, moving from simpler and idealized conditions to more realistic ones and demonstrating the influence of magnetic field and disorder on the dynamic properties of these crystals.

1. Magnetic field $B = 0$, no disorder.

Wigner crystal in the absence of magnetic field and disorder has two branches of phonon phonon vibrations: longitudinal (plasmons) L and transverse T [10].

$$\omega_L(q) = (ne^2 q/2m\varepsilon)^{1/2},$$
$$\omega_T(q) = c_t q = (\beta/nm)^{1/2} q, \qquad (1)$$
$$\beta = (0.245 n^{3/2} e^2/4\pi\varepsilon),$$

where q is the wave vector, n is the electron concentration, e — electron charge, m — electron mass (see Fig. 1).

2. Magnetic field $B \neq 0$, no disorder.

In a magnetic field, Lorentz forces mix the modes ω_L and ω_T. Two hybrid modes with frequencies частотами ω_+ and ω_- [11] appear:

$$\omega_\pm = \frac{1}{2}(\omega_L^2 + \omega_T^2 + \omega_c^2) \pm$$
$$\pm \frac{1}{2}\sqrt{(\omega_L^2 + \omega_T^2 + \omega_c^2)^2 - 4\omega_L^2 \omega_T^2}\,, \qquad (2)$$

where $\omega_c = eB/mc$ is cyclotron frequency, B is magnetic field. Under the condition $\omega_c \gg \omega_L$, ω_T (in strong magnetic field) ω_+ — magnetoplasmon mode (with gap formation), ω_- — magnetophonon mode (gapless) appear (see Fig. 2)

$$\omega_+(q) = \omega_c + \omega_L^2(q)/\omega_c,$$
$$\omega_-(q) = \omega_L(q)\omega_T(q)/\omega_c \propto q^{3/2}. \qquad (3)$$

3. Magnetic field $B \neq 0$, disorder is present.

In the presence of disorder, the classical triangular lattice of the Wigner crystal deforms and loses long-range order. The Wigner crystal breaks down into domains that are pinned to crystal defects with a finite correlation length (domain size) – a Wigner glass. In the presence of disorder, the frequency ω_- changes, a gap appears equal to $\hbar\omega_{PK}$ (see Fig. 3), where ω_{PK} is the pinning frequency,

$$\omega_- = (1/\omega_c)\sqrt{(\omega_{p0}^2 + \omega_L^2(q))(\omega_{p0}^2 + \omega_T^2(q))}, \qquad (4)$$

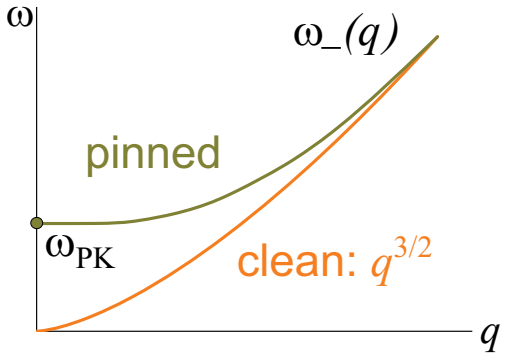

Fig. 3. Disordered two-dimensional Wigner crystal in a perpendicular magnetic field: magnetophonon mode with a gap (pinning mode). Magnetoplasmon mode is not shown

where ω_{p0} is the pinning frequency at $B = 0$, at $q \sim 0$. It is at this frequency $\omega_{PK} = \omega_{p0}^2/\omega_c$ that the maximum power absorption is observed when studying the frequency dependencies Re σ_{xx} in a magnetic field [11, 12].

The dynamic response of a weakly pinned Wigner crystal is controlled by collective excitations, resulting in an absorption line called the pinning mode. These are collective vibrations of correlated segments around equilibrium positions formed by the inhomogeneous pinning potential. These modes have been successfully studied in experimental works [9, 13] using microwave spectroscopy techniques. However, they mainly investigated frequency dependencies of only the real component of high-frequency conductivity.

To interpret our results, we used work [14]. In this work, based on the concepts outlined above, the authors determined the frequency dependencies of Wigner glass conductivity.

The character of the frequency dependence of Wigner glass conductivity depends on the relationship between the parameters of the Wigner crystal, structural disorder, and magnetic field strength. Analysis of this dependence in the general case is not possible. However, when conditions are met

$$1 < \eta < \omega_c/\omega_{p0}, \quad l_B \ll \xi \approx L, \tag{5}$$

where $\eta = \sqrt{\lambda/\beta}$ (λ — bulk, β — shear elastic moduli of the Wigner crystal), $l_B = \sqrt{\hbar c/eB}$ — magnetic length, L — correlation length (size) of the Wigner domain, ξ disorder correlation length. The formula for the frequency dependence of conductivity significantly simplifies:

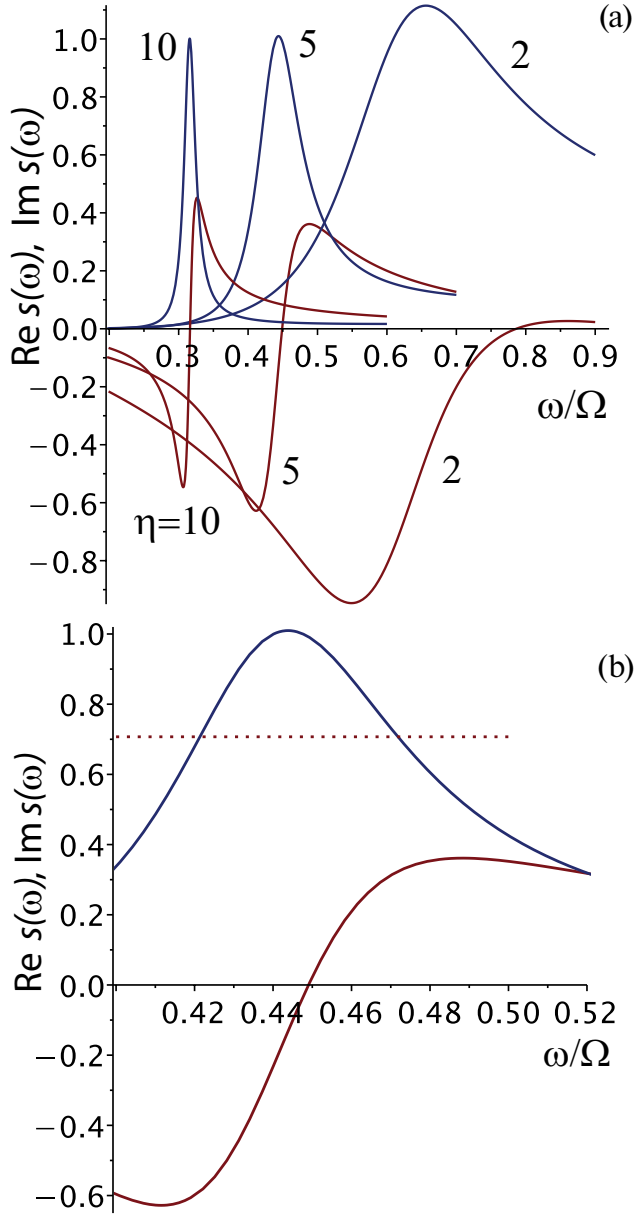

Fig. 4. Dependencies of Re s and Im s on $\varpi = \omega/\Omega$ for different η (*a*) and for $\eta = 5$ (*b*)

$$\sigma(\omega) = -i\frac{e^2 n\omega}{m^* \omega_{p0}^2} \frac{1 - iu(\omega)}{[1 - iu(\omega)]^2 - (\omega\omega_c/\omega_{p0}^2)^2}, \tag{6}$$

ω_{p0} — pinning mode frequency at $B = 0$:

$$u(\omega) \approx \left(\frac{\omega}{\Omega}\right)^3, \omega \ll \Omega, \tag{7}$$

$\Omega \approx \omega_{p0}^2 \eta/\omega_c$. Equation (6) can be reduced to the form

$$\sigma(\omega) \equiv \sigma_0 s\left(\frac{\omega}{\Omega}\right), \text{ where } \sigma_0 = \frac{e^2 n\eta^2}{2m^* \omega_c}, \tag{8}$$

$$s(\varpi) = -2\frac{i\varpi(1-i\varpi^3)}{\eta[(1-i\varpi^3)^2-(\eta\varpi)^2]}, \quad (9)$$

where $\varpi = \omega/\Omega$.

Fig. 4 shows the dependence of s on the reduced frequency ϖ at several values of parameter η.

The Larkin length, i.e., the correlation length (size) of the Wigner crystal domain is determined by the formula

$$L = 2\pi c_t/\omega_{p0}, \quad (10)$$

where $c_t = (\beta/nm^*)^{1/2}$ is the transverse mode velocity of the Wigner crystal.

The theoretical studies presented above of the frequency (dynamic) properties of the Wigner crystal in two-dimensional structures at low temperatures in strong magnetic fields have shown that acoustic studies can be very useful in this field, as they allow determining the real and imaginary components of high-frequency conductivity $\sigma^{hf} = \sigma_1 - i\sigma_2$.

3. EXPERIMENTAL RESULTS

In this work, acoustic methods were used to study the dynamic characteristics of twodimensional structures in the Wigner crystallization regime. The principle of these methods is that the studied sample with 2D conductivity was pressed by a spring to the surface of a lithium niobate piezoelectric crystal, along which a surface acoustic wave (SAW) propagated with two-dimensional conductivity (see Fig. 5). (No deformation was transmitted to the sample.) The electric field accompanying the SAW penetrated into the quantum well of the structure and interacted with charge carriers. As a result of this interaction, SAW absorption and velocity change occurred. The entire system was immersed in a cryostat with a superconducting magnet. SAWs were created on the lithium niobate surface using interdigital transducers with a fundamental frequency of 28 MHz. Measurements of SAW absorption and velocity change were carried out at harmonics with frequencies of 86 MHz, 142 MHz, 197 MHz, 252 MHz, and 306 MHz in magnetic fields up to 18 T and temperatures of 20–400 mK.

The objects of study were structures n-GaAs/AlGaAs, p-GaAs/AlGaAs and p-Si/GeSi with high mobility.

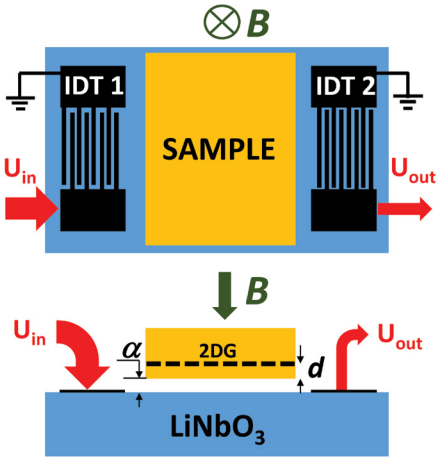

Fig. 5. Experimental setup

According to [15], the absorption and SAW velocity are related to conductivity by the following formulas:

$$\Gamma\left[\frac{\text{dB}}{\text{cm}}\right] = 8.68\frac{K^2}{2}qA \times \times \frac{4\pi\sigma_1\, t(q)/\varepsilon_s v}{[1+4\pi\sigma_2\, t(q)/\varepsilon_s v]^2 + [4\pi\sigma_1\, t(q)/\varepsilon_s v]^2} \quad (11)$$

$$A = 8\, b(q)(\varepsilon_1+\varepsilon_0)\,\varepsilon_0^2\varepsilon_s \exp[-2q(\alpha+d)], \quad (12)$$

$$\frac{\Delta v}{v_0} = \frac{K^2}{2}A \times \times \frac{1+4\pi\sigma_2\, t(q)\,/\,\varepsilon_s v}{[1+4\pi\sigma_2\, t(q)/\varepsilon_s v]^2 + [4\pi\sigma_1\, t(q)/\varepsilon_s v]^2}, \quad (13)$$

$$b(q) = (b_1(q)[b_2(q)-b_3(q)])^{-1},$$

$$t(q) = [b_2(q)-b_3(q)]/2b_1(q),$$

$$b_1(q) = (\varepsilon_1+\varepsilon_0)(\varepsilon_s+\varepsilon_0) - -(\varepsilon_1-\varepsilon_0)(\varepsilon_s-\varepsilon_0)e^{(-2q\alpha)},$$

$$b_2(q) = (\varepsilon_1+\varepsilon_0)(\varepsilon_s+\varepsilon_0) + +(\varepsilon_1+\varepsilon_0)(\varepsilon_s-\varepsilon_0)e^{(-2qd)},$$

$$b_3(k) = (\varepsilon_1-\varepsilon_0)(\varepsilon_s-\varepsilon_0)e^{(-2q\alpha)} + +(\varepsilon_1-\varepsilon_0)(\varepsilon_s+\varepsilon_0)e^{[-2q(\alpha+d)]},$$

where Γ and $\Delta v/v_0$ are the absolute change in absorption and relative change in SAW velocity in

magnetic field, v is the SAW velocity in lithium niobate in magnetic field, v_0 is the sound velocity at $B = 0$, K^2 — electromechanical coupling constant of $LiNbO_3$, q is the wave vector, d is the embedding depth of the two-dimensional layer, $\varepsilon_1 = 50$, $\varepsilon_0 = 1$ and $\varepsilon_s = 11$ are the dielectric constants of lithium niobate, vacuum, and semiconductor respectively. The distance between lithium niobate and the studied structure $\alpha \approx 5 \cdot 10^{-5}$ cm was determined from the SAW velocity saturation value in strong magnetic field. Simultaneous solution of equations (11) and (13) allows calculating the values of real and imaginary components of high-frequency conductivity σ_1 and σ_2.

3.1 *n*-GaAlAs/GaAs/GaAlAs [16]

The frequency properties of high-frequency conductivity corresponding to Wigner glass were most prominently manifested in *n*-GaAlAs/GaAs/GaAlAs structures with low electron concentration $n = 5 \cdot 10^{10}$ cm^{-2} and high mobility $8 \cdot 10^6$ cm^2/V $\cdot$ s in magnetic fields corresponding to filling factors from 0.19 to 0.125 in the temperature range of 40–380 mK (Fig. 6). The well width was 65 nm, in this range of magnetic fields $\kappa_s = 11$–13.

As shown in Fig. 7, at all magnetic fields, the frequency dependence of real and imaginary components of high-frequency conductivity demonstrates behavior corresponding to the regime of Wigner crystal domain formation in structures. Moreover, the higher the magnetic field (lower ν), the smaller the value of maximum real conductivity component. The dependencies of σ_1 value on frequency for different ν are presented in Fig. 8. The dependence $\sigma_1^{max} \propto \omega_c^{-1}$ (see inset in Fig. 8) is confirmed by theory (formula (8)).

The frequency dependence σ_1 and σ_2 for the studied sample at $\nu = 0.18$ qualitatively coincides with the theoretical curves shown in Fig. 4 for $\eta = 5$. This means that the maximum σ_1 occurs at $\omega^{max}/2\pi \approx 86$ MHz at $\omega/\Omega = 0.44$, thus, $\Omega \approx 1.2 \cdot 10^9 \text{s}^{-1}$. According to the formulas in work [14]

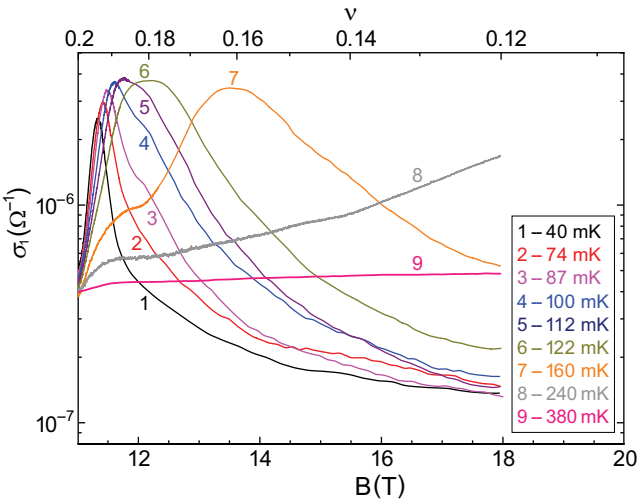

Fig. 6. Dependence of σ_1 on magnetic field at different temperatures, $f = 28.5$ MHz

$$\omega_{p0} = \sqrt{\omega_c \Omega/\eta} = 8.7 \cdot 10^{10} \text{s}^{-1} \qquad (14)$$

is the pinning frequency at $B = 0$;

Let's determine the domain correlation length (its size) using formula (10):

$$L = 2\pi c_t/\omega_{p0} = 3 \cdot 10^{-4} \text{cm}. \qquad (15)$$

This means that the conditions necessary for using the formulas from work [14] are met:

$$L \gg a \gg l_B, \qquad (16)$$

where a is the distance between electrons in the structure ($2.5 \cdot 10^{-6}$ cm), and $l_B = 7.3 \cdot 10^{-7}$ cm is the magnetic length at $B = 12.2$ T; furthermore, this allows us to conclude that the Wigner crystal domain includes on average about 100 electrons.

The numerical calculations presented here are only approximate, as working with SAW harmonics does not allow precise determination of the maximum in the conductivity frequency dependence.

From the set of experimental curves shown in Fig. 6, one can construct the dependence of the real component of high-frequency conductivity on temperature at different magnetic fields (Fig. 9).

In Fig. 9, it can be seen that for each filling factor, there is a maximum in the real component of conductivity versus temperature. To the left of the maximum, the temperature dependence can

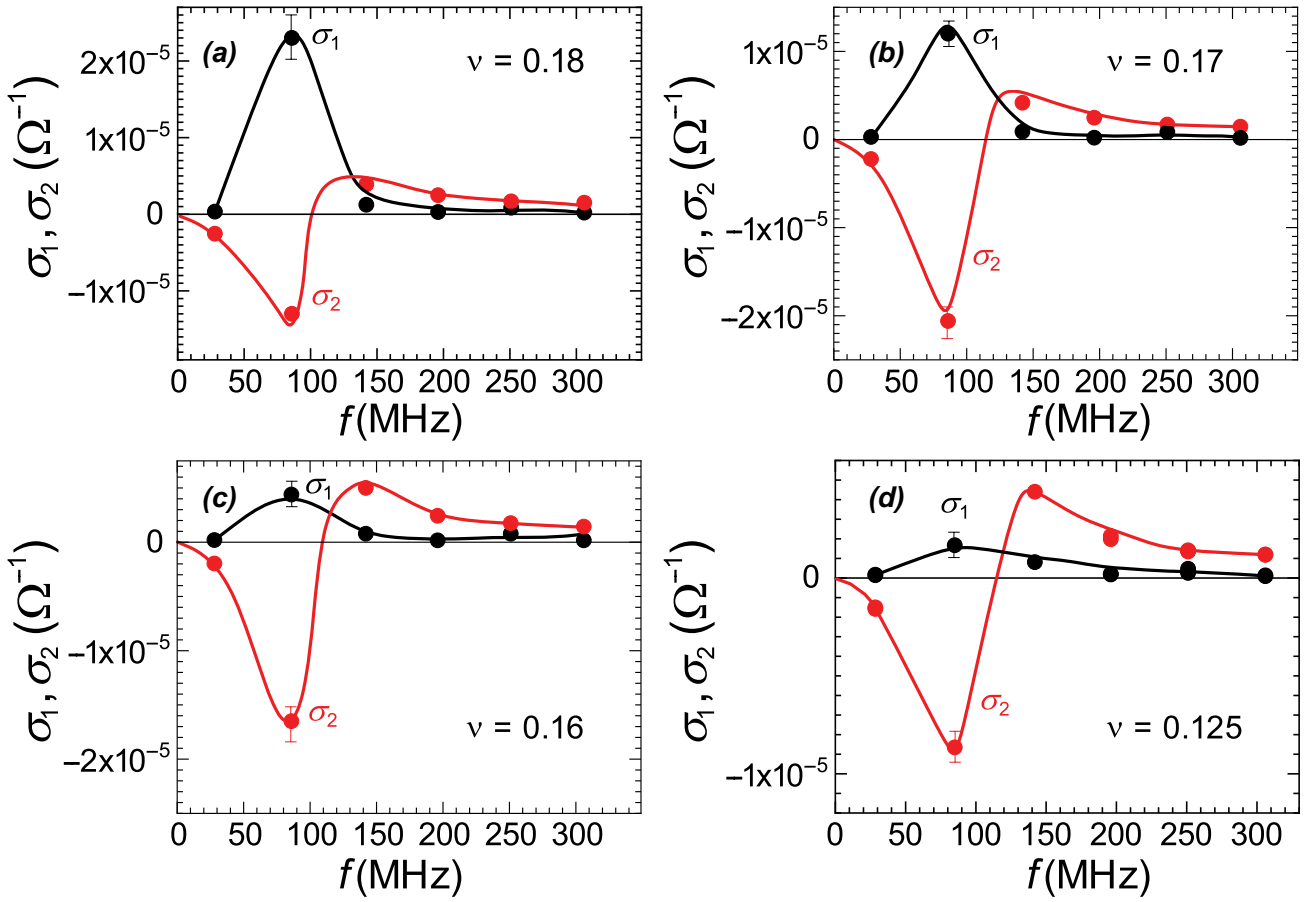

Fig. 7. Frequency dependencies of σ_1 and σ_2 for different ν: 0.18 ($B = 12.2$ T), 0.17 ($B = 13$ T), 0.16 ($B = 13.6$ T) and 0.125 ($B = 17.6$ T); $T = 40$ mK

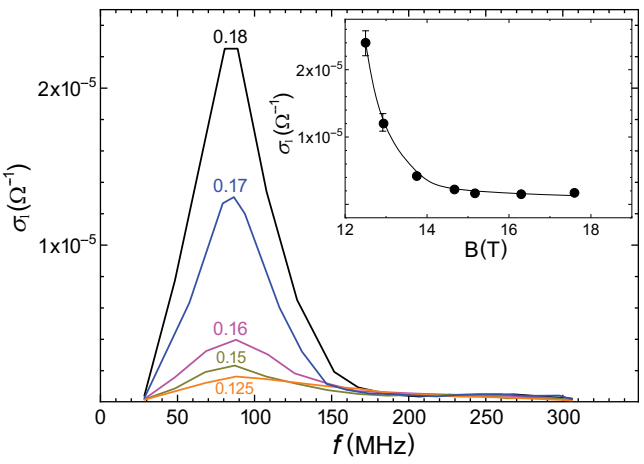

Fig. 8. Dependencies of σ_1 on frequency f for different ν. Inset: dependence of σ_1^{max} on magnetic field; $T = 40$ mK

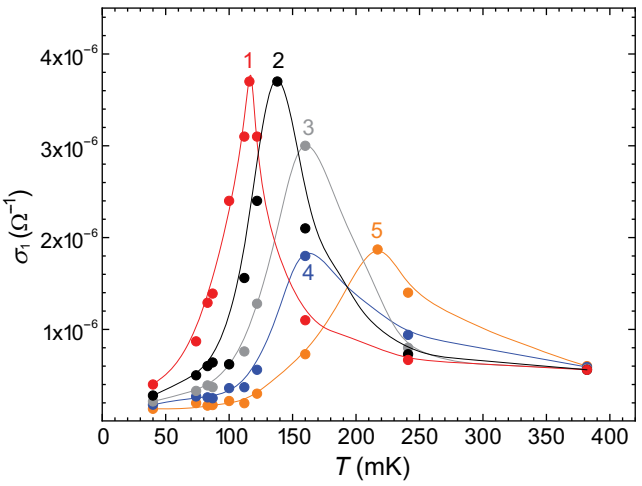

Fig. 9. Temperature dependence of σ_1 at different filling factors ν: *1* —0.18, *2* —0.17, *3* — 0.16, *4* — 0.145, *5* — 0.125; $f = 28.5$ MHz

be described by the Arrhenius law. The activation energies calculated from the dependencies $\ln \sigma_1(1/T)$ increase with increasing magnetic field (Fig. 10*a*), then tend to saturation (Fig. 10*b*).

We believe that such dependencies characterize the Wigner glass region. To the right of maximum conductivity sharply decreases with increasing temperature – the temperature dependence of

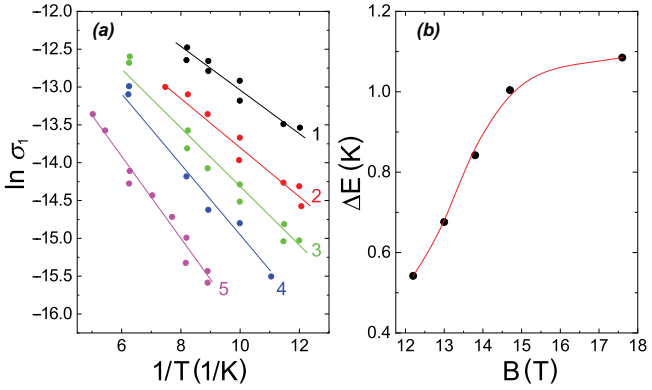

Fig. 10. *a* — Dependencies of ln σ_1 on $1/T$ for different filling factors ν: *1* —0.18, *2* —0.17, *3* — 0.16, *4* — 0.145, *5* — 0.125; from the dielectric conductivity side (before the maximum σ_1). *b* — Dependence of activation energy ΔE on magnetic field

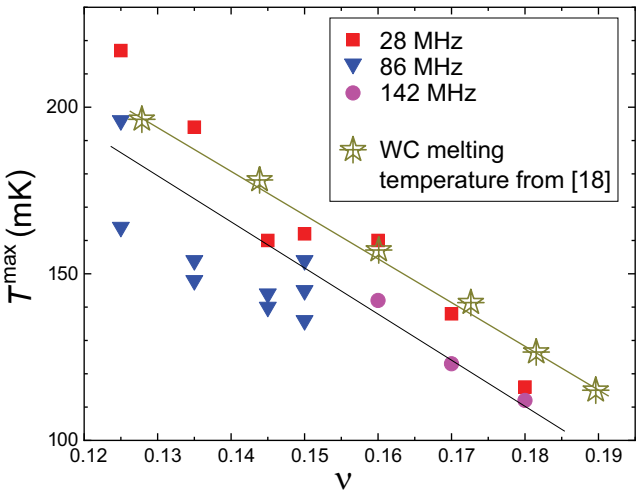

Fig. 11. Dependence of T^{max} on filling factor ν for different frequencies 28.5 MHz, 86 MHz and 142 MHz and the melting temperature, determined later in [18] in a structure with a 70 nm GaAs quantum well with $n = 4.2 \cdot 10^{10}$ cm^{-2}

conductivity becomes metallic-like. A dielectric-metal transition occurs, and the temperature at which the conductivity maximum occurs in this case characterizes the temperature of Wigner glass melting. Fig. 11 shows the dependence of Wigner glass melting temperature on the filling factor (magnetic field).

In this structure, Wigner glass formation is also observed near filling factors 1/5 [17], 1 and 2 [19], although in these magnetic fields $\kappa_s = 4.5 - 3$.

3.2. *p*-AlGaAs/GaAs/AlGaAs [20]

High-frequency conductivity measurements were also performed in the structure *p*-GaAs/AlGaAs with concentration $p = 1.2 \cdot 10^{11}$ cm^{-2} and mobility $1.8 \cdot 10^6$ cm^2/V$\cdot$s in the temperature range 20–300 mK, frequency 28.5–306 MHz and magnetic fields up to 18 T.

In Fig. 12, it can be seen that near filling factors 1 and 1/3 there are anomalous conductivity surges in the form of asymmetric maxima, "wings".

Fig. 13 shows temperature dependencies of the real part of conductivity at fixed magnetic fields. In this figure, it can be seen that in a magnetic field of 6.6 T at a temperature of about 110 mK, there is a conductivity maximum that shifts toward lower temperatures as the magnetic field increases to 7.0 T. To the left of the maximum at $\nu = 1$ carriers are activated to the mobility edge from localized states $\nu = 1$. To the right of the maximum, conductivity becomes metallic-type. And only in a small range of magnetic fields 7.0–7.2 T the frequency dependence of conductivity has the form shown in Fig. 14.

In Fig. 14, it can be seen that compared to the previous structure (*n*-AlGaAs/GaAs/AlGaAs) this dependence only resembles the frequency dependence of conductivity in well-developed Wigner glass. Therefore, we assume that such frequency dependence of real σ_1 and imaginary σ_2 components of high-frequency conductivity in the anomaly region is associated with the coexistence of two phases: Wigner glass and Fermi liquid of delocalized charge carriers [21].

Similar frequency dependencies of the imaginary component σ_2 of high-frequency conductivity are also observed near other anomalies that occur near filling factors characteristic of the fractional quantum Hall effect: $\nu = 2/3, 2/5, 1/3$ (see Fig. 15), which suggests that near each conductivity maximum (see Fig. 12) there is a small region in magnetic field where two phases coexist: Wigner glass and Fermi liquid.

3.3. *p*-Si/SiGe/Si [22]

High-frequency conductivity was also studied in the structure *p*-Si/SiGe/Si with concentration $p = 8 \cdot 10^{10}$ cm^{-2} and hole mobility $1 \cdot 10^4$ cm^2/V$\cdot$s in the temperature range (0.3–4.2) K in magnetic fields up to 18 T and SAW frequencies (18–255) MHz.

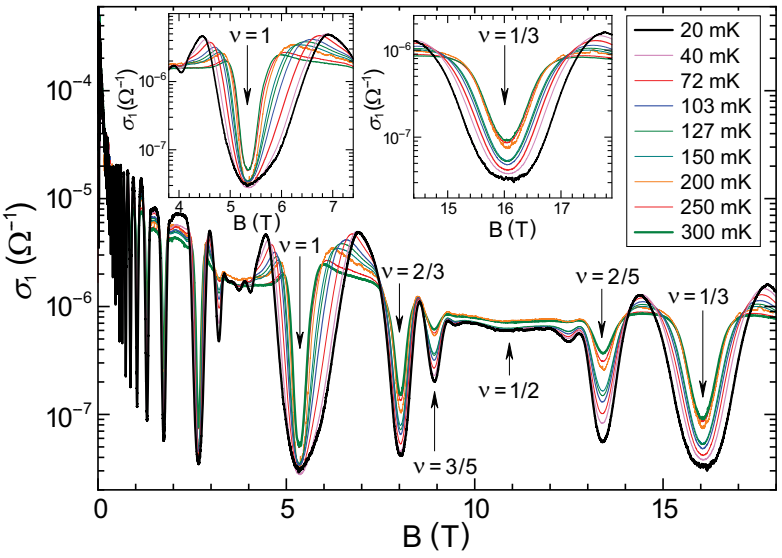

Fig. 12. Dependence of the real component of conductivity σ_1 on magnetic field at different temperatures, $f = 86$ MHz. Insets show the dependence of σ_1 on magnetic field near filling factors 1 (*a*) and 1/3 (*b*)

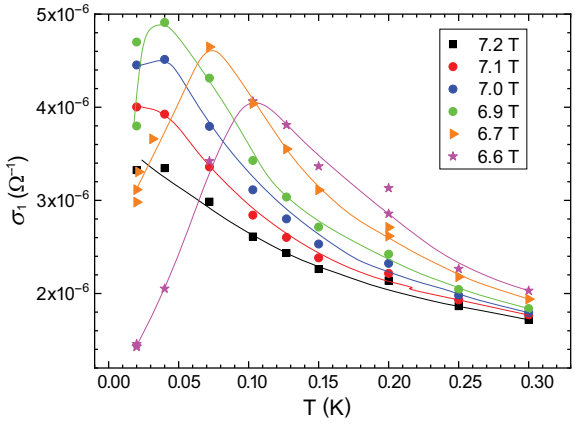

Fig. 13. Dependence of σ_1 on temperature at different magnetic field values in the conductivity anomaly regions ("wings")

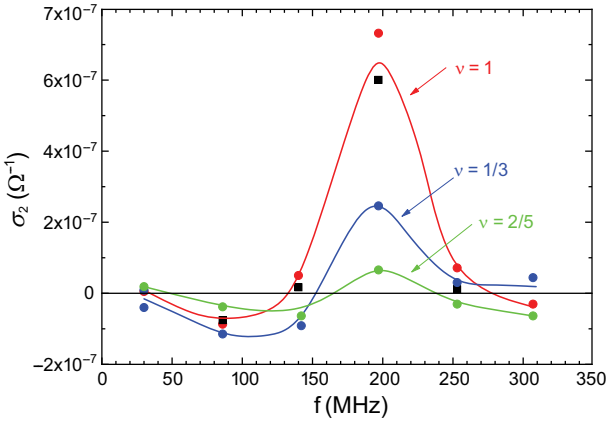

Fig. 15. Frequency dependencies of the imaginary component of conductivity σ_2 near different filling factors ν ($\kappa_s = 20$ for $\nu = 1$, $\kappa_s = 31$ for $\nu = 2/5$, $\kappa_s = 33$ for $\nu = 1/3$)

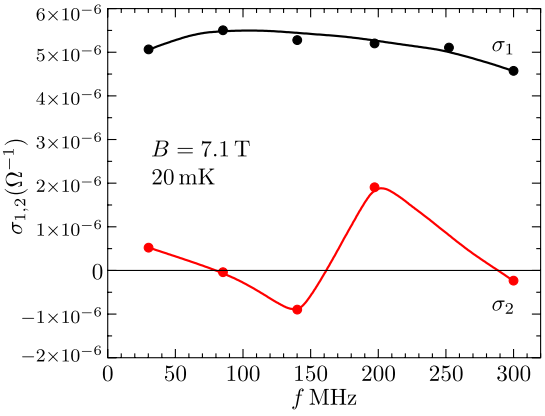

Fig. 14. Dependence of σ_1 and σ_2 on frequency at $T = 20$ mK, $B = 7.1$ T near $\nu = 1$ ($\nu = 0.76$)

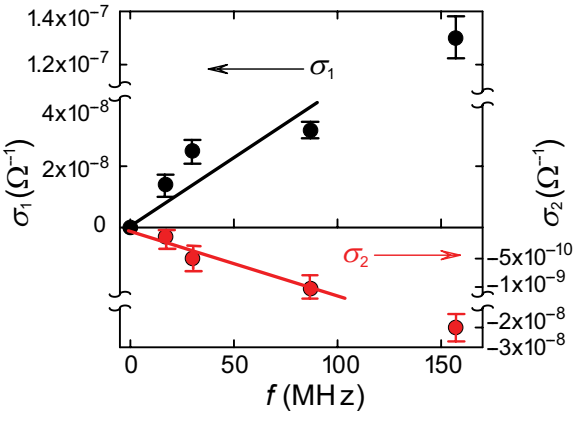

Fig. 16. Dependence of σ_1 and σ_2 on frequency f at $T = 300$ mK and $B = 18$ T

At $T = 300$ mK in this structure, an unusual frequency dependence of components σ_1 and σ_2 (see Fig. 16) was observed.

The negative sign of the imaginary part of conductivity shown in Fig. 16 could only be explained by the formation of islands (domains) of Wigner crystal, pinned on disorder away from the pinning frequency. Indeed, based on work [14], away from the pinning frequency, under the condition

$$u \gg \omega\omega_c/\omega_{p0}^2 \gg 1 \tag{17}$$

the conductivity is determined by equations

$$\begin{aligned} \mathrm{Re}\ \sigma_{xx} = \sigma_1 &= \frac{e^2 p}{m^* \omega_{p0}^2}\frac{\omega}{u}, \\ \mathrm{Im}\ \sigma_{xx} = \sigma_2 &= -\frac{e^2 p}{m^* \omega_{p0}^2}\frac{\omega}{u^2}. \end{aligned} \tag{18}$$

Since the experiment showed a linear dependence of σ_1 and σ_2 on frequency, it was possible to determine the value of $u = 40$. This means that condition (17) is satisfied, which allows estimating the pinning frequency in the absence of magnetic field $\omega_{p0} \approx 1.5 \cdot 10^{10}$ s^{-1}.

Now the value of u is known from the experiment and the estimate of ω_{p0}, has been made, therefore, using formula (18), one can determine the concentration of holes p_{WC}, forming the Wigner crystal domains and their average size L using formula (10). It turned out that $p_{WC} \approx 10^9$ cm^{-2}, and $L \approx 4 \cdot 10^{-4}$ cm.

4. CONCLUSIONS

In two-dimensional structures with high mobility (low disorder) and low charge carrier

concentration at temperatures 20–300 mK in strong magnetic field, there is a high probability of observing the formation of Wigner crystal domains – Wigner glass. Acoustic methods are very useful for detecting and studying the parameters and dynamic properties of this state.

ACKNOWLEDGMENTS

The authors are grateful to E. Green, R. Nowell and L. Jiao for help in conducting experiments at NHMFL; K. W. Baldwin, L. N. Pfeiffer and K. W. West for provided AlGaAs/GaAs/AlGaAs samples, and to O. Mironov and M. Mironov for providing samples Si/SiGe/Si.

FUNDING

NNHMFL is supported by NSF/DMR-1157490, NSF/DMR-1644779, NSF/DMR-2128556 grants and the state of Florida.

REFERENCES

1. E. P. Wigner, Phys. Rev. **46**, 1002 (1934).
2. A. V. Chaplik, Soviet Physics JETP 35, 395 (1972) [Zh. Eksp. Teor. Fiz. **62**, 746 (1972)].
3. Yu. E. Lozovik, V. I. Yudson, JETP Letters **22**, 11 (1975) [JETP Letters, 22, 26 (1975].
4. C. C. Grimes, and G. Adams, Phys. Rev. Lett. **42**, 795 (1979).
5. M. Shayegan, Nature Rev. Phys. **4**, 212 (2022).
6. M. Shayegan, *Flatland Electrons in High Magnetic Fields, Vol. 3 of High Magnetic Fields: Science and Technology*, World Scientific Co, Singapore (2006), p. 31.
7. V.M. Pudalov, Phys. Quantum Electrons Solid (international, Cambridge, MA (1994) p. 124.
8. M. A. Paalanen, R. L. Willet, P. B. Littlewood et al., Phys. Rev. **45**, 11342 (1992); M. A. Paalanen, R. L. Willet, R. R. Ruel et al., Phys. Rev. B **45**, 13784 (1992).
9. Yong P. Chen, *Quantum Solids of Two Dimensional Electrons in Magnetic Fields*, PhD Thesis, Princeton University (2005), p. 215
10. L. Bonsall and A. A. Maradudin, Phys. Rev.B **15**, 1959 (1977).
11. B. G. A. Normand, P. B. Littlewood, and A. J. Millis, Phys. Rev. B **46**, 3920 (1992).
12. H. Fukuyama, and P. A. Lee, Phys. Rev.B **17**, 535 (1978).
13. P.D. Ye, L. W. Engel, D. C. Tsui et al., Phys. Rev. Lett. **89**, 176802 (2002).
14. M. M. Fogler and D. A. Huse, Phys. Rev. B **62**, 7553 (2000).
15. I. L. Drichko, A. M. Diakonov, I. Y. Smirnov et al., Phys. Rev. B **62**, 7470 (2000).
16. I. L. Drichko, I. Yu. Smirnov, A.V. Suslov et al., Phys. Rev. B **94**, 075420 (2016).
17. I. L. Drichko, I. Yu. Smirnov, A. V. Suslov et al., Solid State Commun. **213-214**, 46 (2015).

18. H. Deng, L. N. Pfeiffer, K.W.West et al., Phys. Rev. Lett. 122, 116601 (2019).

19. I. L. Drichko, I. Yu. Smirnov, A. V. Suslov et al., Phys. Rev. B **92**, 205313 (2015).

20. I. L. Drichko, I. Yu. Smirnov, A. V. Suslov et al., Phys. Rev. B **107**, 085301 (2023).

21. V. M. Pudalov, JETP Letters **116**, 456 (2022).

22. I. L. Drichko, A. M. Dyakonov, I. Yu. Smirnov et al., Phys. Rev. B **77**, 085327 (2008).